

## Simulation of starting/stopping vortices for a lifting aerofoil

M. Vincent and H. M. Blackburn

Department of Mechanical and Aerospace Engineering  
 Monash University, Victoria 3800, Australia

### Abstract

In order to recreate Prandtl's flow visualisation films dealing with starting and stopping vortices produced by a lifting aerofoil and expand on that research, direct numerical simulation was used to perform numerical experiments on the starting and stopping of lifting aerofoil by solving the two-dimensional incompressible Navier–Stokes equations. The simulation used a NACA 0012 aerofoil at angle of attack  $\alpha = 4^\circ$ , the chord Reynolds number based on peak translation speed was  $Re = 10\,000$ , and was conducted using a spectral element simulation code. Trailing edge starting and stopping vortices and also a stopping leading edge vortex pair were produced. Net circulation was calculated and was found to have a small positive value, which fell as domain size was increased. The circulation agreed with the domain integral vorticity as expected. We examined the aerodynamics of the aerofoil by calculating the lift and drag coefficients and the lift-to-drag ratio. We found that  $C_D$  was larger than  $C_L$  when the aerofoil was accelerating and decelerating, but smaller during steady state velocity. Most of the drag was associated with pressure gradients as opposed to viscous skin friction. Details of circulation/vorticity generation and evolution will be presented.

### Introduction

Prandtl, Tietjens and Müller recorded the motion of fine particles sprayed across the surface of a water channel to visualize the flow around obstacles more than 80 years ago.[1] A snapshot of the flow around a lifting aerofoil that has been impulsively started, then brought to rest, can be seen in Figure 1. Starting and stopping vortices can be seen adjacent to the trailing edge. A starting vortex is formed and is washed away with the fluid. When the aerofoil stops, a stopping vortex is produced. The pair of vortices then propel each other downwards.

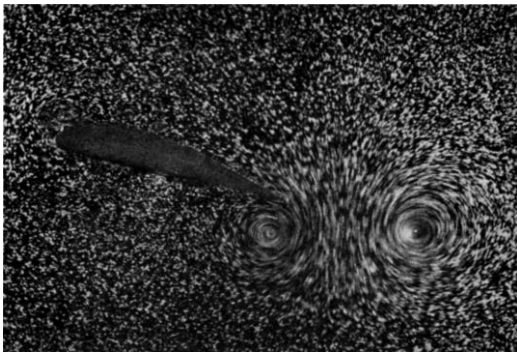


Figure 1. Snapshot from Prandtl's historic flow visualisation film of the transient lifting aerofoil.[1][3]

More recently, Lei, Feng and Can (2013) found that at a low Reynolds number, laminar separation occurred in the flow field around a symmetrical aerofoil and when the angle of attack reached a certain level, primary and secondary vortices were produced.[4] Jones and Babinsky (2011) found that leading edge vortices were shed from the flat plates at  $Re=10000-60000$ . [5] Sun and Daichin (2011) looked at wing tip vortices and found that the vorticity decreased with decreasing ground height.[6]

In the present work, Prandtl's experiment was numerically recreated by solving the two-dimensional incompressible Navier–Stokes equations in an accelerating reference frame

$$\partial_t \mathbf{u} + \mathbf{u} \cdot \nabla \mathbf{u} = -\rho^{-1} \nabla p + Re^{-1} \nabla^2 \mathbf{u} - \mathbf{a}, \quad \nabla \cdot \mathbf{u} = 0, \quad (1)$$

where  $\mathbf{a}$  is the frame acceleration and  $Re = \tilde{U}c/\nu$  is the Reynolds number.  $\tilde{U}$  is the peak translational velocity and  $c$  is the chord length. Hence, the normalised time is  $t = c/\tilde{U}$ . We aim to simulate a lifting NACA0012 aerofoil to observe the flow around the aerofoil; in particular the starting and stopping vortices, build and expand on the past research, and also look at the vorticity, pressure distribution and aerodynamics of the aerofoil by calculating the circulation and lift and drag coefficients.

A starting vortex is shed owing to viscous friction on the surface of the aerofoil that causes the large velocity round the trailing edge to develop into a surface discontinuity and the aerofoil to discharge vorticity into the fluid. When the aerofoil comes to rest, a stopping vortex is shed, consistent with Thompson's theorem and Kelvin's theorem. Vorticity and circulation can be related via Stokes' theorem [7]:

$$\int \boldsymbol{\omega} \cdot d\mathbf{S} = \Gamma = \oint \mathbf{u} \cdot d\mathbf{l}. \quad (2)$$

In order to calculate the vorticity source strength at the walls of the aerofoil in an inertial reference frame, we use the equation:

$$-v\mathbf{n} \cdot \nabla \boldsymbol{\omega} = -\mathbf{n} \times (\nabla \mathbf{P} + \mathbf{a}), \quad (3)$$

where  $\boldsymbol{\omega}$  is the vorticity vector,  $\mathbf{n}$  is a unit wall-normal vector and  $\mathbf{a}$  is the wall acceleration.[8] As using a reference frame with the aerofoil at rest in a moving fluid or with the aerofoil in motion in a stationary fluid produces the same vorticity, in the present application we could assume that the pressure gradient associated with transient motion is small compared to the aerofoil's acceleration and produce a first-order estimate of the vorticity production around the surface of the aerofoil using

$$-v\mathbf{n} \cdot \nabla \boldsymbol{\omega} = -\mathbf{n} \times \mathbf{a} = \mathbf{t} \cdot \mathbf{a}, \quad (4)$$

where  $\mathbf{t}$  is the unit tangent vector. This method, though rather crude, has the advantage of only requiring the aerofoil's geometry and acceleration.

## Methodology

Two-dimensional flow past a NACA 0012 aerofoil at 4 degrees angle of attack was simulated using a spectral element simulation code.[2] The mesh has 891 spectral elements and is illustrated in figure 2. The simulation domain had a total normalised area of  $17.5c^2$ . Within each spectral element, tensor-product basis functions of fourth order were used, giving a total of 14,366 independent mesh nodes.

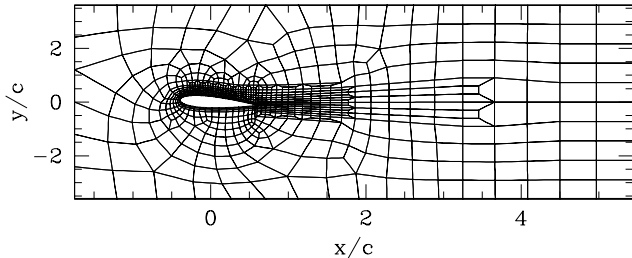


Figure 2. Spectral element mesh for the NACA 0012 aerofoil.

Body forces and boundary conditions were implemented to produce starting and stopping of the aerofoil by moving fluid past the aerofoil, similarly to previous applications.[9] The aerofoil's horizontal translational velocity increased smoothly to unity, remained at steady state for a while, and then smoothly decreased until the aerofoil was at rest again, travelling a total distance of one chord length. The simulation was made to run for until  $t = 30$ , with the aerofoil coming to rest at  $t = 1$ . While it is not now easy to check the Reynolds number obtained in the original experiments, a simulation Reynolds number of 10,000 was found sufficient to produce concentrated starting and stopping vortices. The results were post processed to produce animations of the vorticity field of the aerofoil. Plots of the vorticity and pressure contours were obtained.

In order to validate the data, the convergence of the results was demonstrated using Stokes's Theorem. Circulation calculations were verified using the Law of Kutta-Joukowski. Circulations of the starting and stopping vortices were also calculated individually and compared to ensure they were equal and opposite. The lift and drag coefficients, and the lift-to-drag ratio were calculated. The coefficients of drag due to pressure and viscosity were calculated separately and compared. After obtaining all results, it was decided to increase the domain of the mesh in order to obtain a more accurate conservation of circulation. Using the same aerofoil, the domain area was later increased to  $60c^2$  and the process of producing the animations and calculating the circulation and integral of vorticity were repeated.

## Force coefficients

The transient lift and drag coefficients for the aerofoil, based on the integrated total forces and peak translational speed, are shown in figure 3.

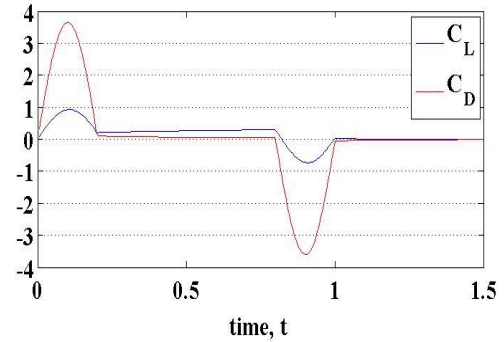


Figure 3. Evolution of  $C_L$  and  $C_D$  based on peak translational speed.

The shape of the drag coefficient plot closely follows the acceleration profile used (two half-cosine waves) and is dominated by added-mass effects. The lift coefficient also shows added-mass effects, but grows with time during the intermediate period of steady speed, before eventually falling to zero after the aerofoil is brought to rest. Assuming a lift-curve slope  $\partial C_L / \partial \alpha = 2\pi$ , the expected steady-state value of coefficient of lift is 0.438, in reasonable agreement with the value seen at  $t = 0.8$ . It is remarkable that forces for this transient flow are dominated by acceleration effects. Note that positive and negative values are observed for both lift and drag.

The drag coefficient may be decomposed into viscous and pressure contributions, as shown in figure 4. As might be expected from the apparent dominance of added-mass effects, pressure drag is far larger than viscous drag during this transient stage.

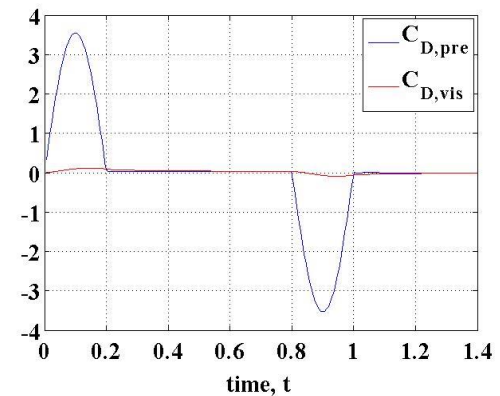


Figure 4. The evolution of the pressure and viscous drag coefficients.

Finally in this section, we show the ratio of lift to drag forces in figure 5. During the initial acceleration and final de-acceleration, the lift to drag ratio is very low, but during the phase of steady translation, the ratio increases monotonically to reach a value of approximately 5.5 before the onset of de-acceleration. Though on first consideration this value may seem surprisingly low, at the comparatively low Reynolds number of  $Re=10,000$ , the steady-state average value of  $L/D$  may not be very large; calculations using XFOIL [10] suggests a value of only 2.68, though one might expect the viscous-inviscid interaction methodology it uses to be unreliable at such low Reynolds numbers.

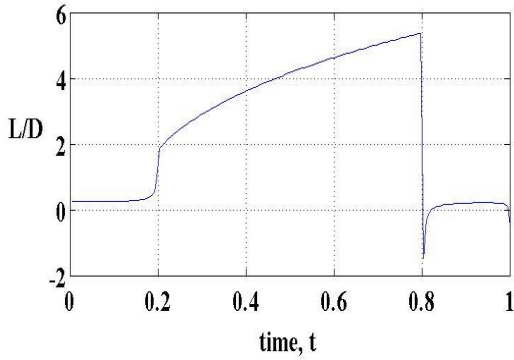


Figure 5. Lift-to-drag ratio as a function of time.

### Vorticity and pressure fields

In figure 6 we present a comparison of vorticity and pressure fields both during and subsequent to the transient motion of the aerofoil. To recapitulate: transient body motion occurs over the interval  $t = 0 - 1$ , with steady translation over the interval  $t = 0.2 - 0.8$ , peak positive and negative accelerations occurring at  $t = 0.1$  and  $t = 0.9$  respectively.

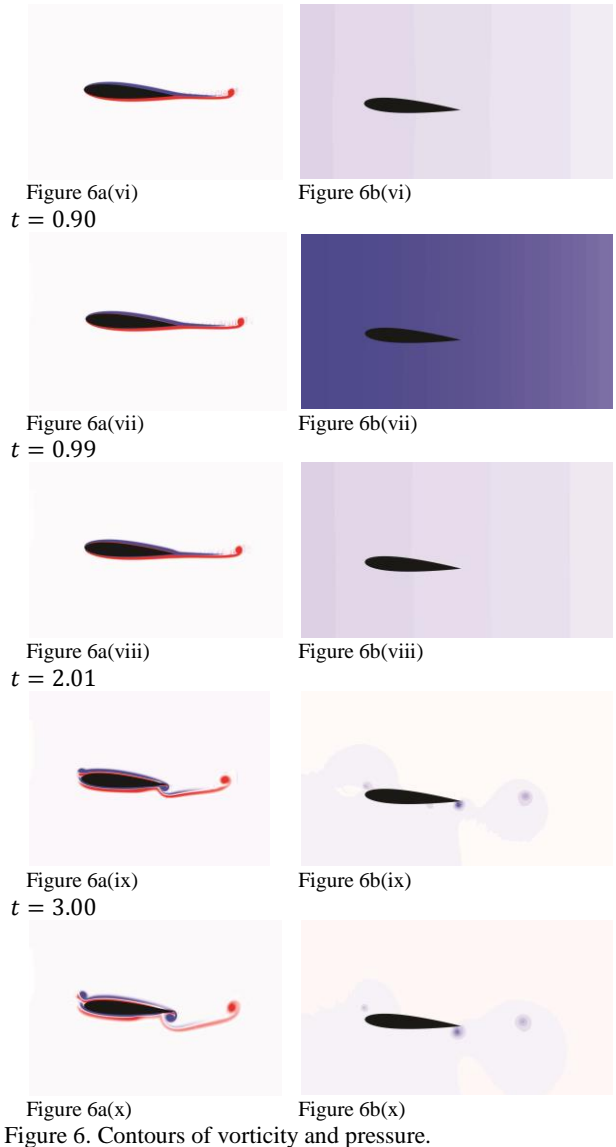
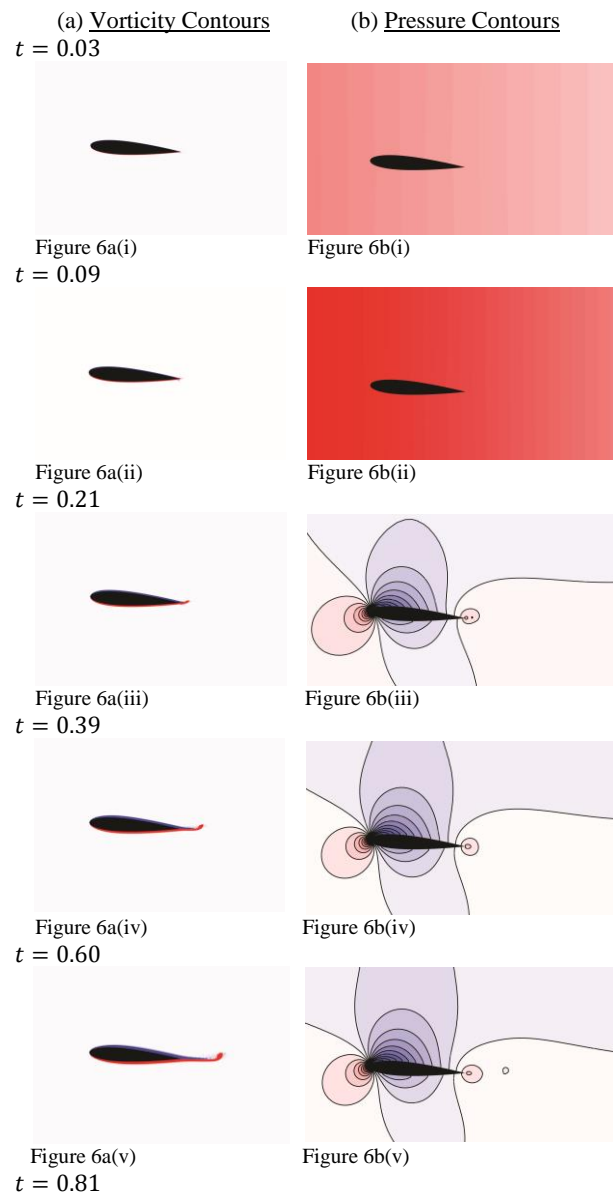


Figure 6. Contours of vorticity and pressure.

From figures 6a(i)-(v), we see that the appearance of a starting vortex is delayed until after the initial acceleration phase and the aerofoil is in steady translation. Similarly, a stopping vortex is only clearly evident well after the aerofoil has come to rest (figures 6a ix and x). The pair of starting and stopping vortices near the trailing edge then are propelled downwards by their opposing motions. The transient lift force thus imparts a downwards momentum to fluid inside the domain.

A leading edge vortex pair is also produced when the aerofoil comes to a rest. There is then also a very thin region of negative vorticity on the upper surface of the aerofoil and a region of positive vorticity on the lower surface.

As can be seen in figures 6b(i)-(x), there is a dominant pressure gradient in the x direction when the aerofoil is accelerating ( $0 \leq t \leq 0.2$ ) and decelerating ( $0.8 \leq t \leq 1$ ) that is maximum at maximum acceleration and deceleration. During steady state velocity, there is a region of low pressure on the upper surface of the aerofoil. There is a region of high pressure at the front of the aerofoil at the stagnation point. There is also a region of (relatively) high pressure that corresponds to the starting vortex, as it evolves from the rear stagnation point.

When the domain extent was later increased, the vorticity and pressure contours were found to be similar to those shown in figure 6.

## Circulation and vorticity

Regardless of Reynolds number, one expects Stokes' theorem to hold, i.e. that the integral of vorticity within a closed loop matches the circulation around it. Figure 7, computed over the entire domain shown in figure 2, demonstrates that the two values do in fact agree at all times, helping to validate our calculations.

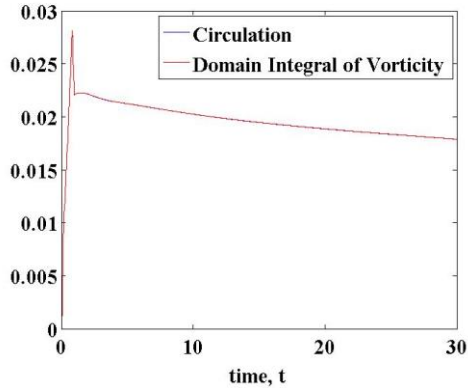


Figure 7. The time histories of the circulation and the domain-integral of vorticity.

However, the circulation around the domain has a small net positive value, peaking at 0.0281, which decreased when the domain was increased. Since the vorticity within the domain is initially zero, one expects the circulation to remain zero provided the domain is made large enough. We checked this by repeating our calculations on a larger domain of area  $60c^2$ . For the larger domain, the graph of the circulation was similar in shape to that shown in figure 7 but with a peak of value 0.0183.

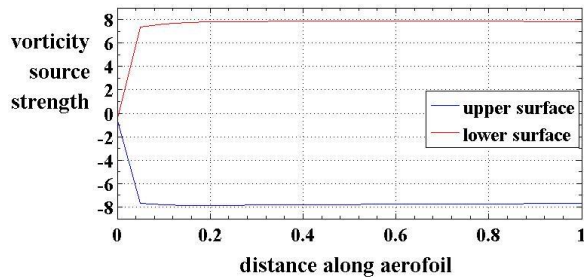


Figure 8. The vorticity source strength along the surface of the aerofoil calculated using (4).

In an initial examination of the generation of vorticity at the aerofoil surface, we have used (4), based on the known frame acceleration and aerofoil geometry to calculate the components of vorticity source strength due just to transient acceleration, with the outcomes shown in figure 8. This shows that vorticity generation is nearly equal and opposite on the two sides of the aerofoil – most of the difference being concentrated over the first 20% of the chord. At the trailing edge, vorticity generation is still large on each side, but with the sum approaching zero. We note that figure 8 agrees with the signs of vorticity evident in figure 6a, with a negative vorticity on the upper surface and a positive vorticity on the lower surface.

## Conclusions

We have successfully simulated the vortices produced during the starting and stopping of a NACA 0012 aerofoil with  $\alpha = 4^\circ$   $Re = 10000$ . Starting and stopping leading and trailing edge vortex pairs were produced. We successfully validated our results, and managed to get the circulation down to a maximum of 0.0183.  $C_D$  was much larger than  $C_L$  when the aerofoil was accelerating and decelerating, with most of the drag due to pressure instead of viscosity. But when the aerofoil was moving with constant velocity,  $C_L$  was larger than  $C_D$ .

In order to expand our research, we could look at the aerodynamics of an aerofoil in a larger domain and with a different mesh. We will also look at the evolution of moment coefficient of the aerofoil.

## References

- [1] National Committee for Fluid Mechanics Films 1972, 'Generation of circulation and lift for an aerofoil. Film loop FM-10', *Illustrated Experiments in Fluid Mechanics*, Semline, Inc., USA.
- [2] Blackburn, H.M. & Sherwin, S.J. 2004, 'Formulation of a Galerkin spectral element–Fourier method for three-dimensional incompressible flows in cylindrical geometries', *J Comp Phys*, vol. 197, no. (2), pp. 759-778
- [3] Prandtl, L & Tietjens, O.G., *Applied Hydro- and Aeromechanics*, Engineering Societies Monographs, 1934. (Dover edition, 1957).
- [4] Lei, J, Feng, G & Can, H 2013, 'Numerical study of separation on the trailing edge of a symmetrical airfoil at a low Reynolds number', *Chinese Journal of Aeronautics*, pp.918-925, Elsevier Ltd., Beijing.
- [5] Jones, A & Babinsky, H 2011, 'Reynolds number effects on leading edge vortex development on a waving wing', *Exp Fluids (2011)*, pp. 197-210, doi: 10.1007/s00348-010-1037-3
- [6] Sun, R & Daichin 2011, 'Experimental Investigation on Tip Vortices and Aerodynamics', *Theoretical & Applied Mechanics Letters 1*, doi: 10.1063/2.1103201
- [7] Tritton, D 1988, *Physical Fluid Dynamics*, 2<sup>nd</sup> edn, Oxford University Press, New York.
- [8] Morton, B. R. 1984 'The generation and decay of vorticity' *Geophys. Astrophys. Fluid Dyn.* 28, 277-308.
- [9] Blackburn H. M. & Henderson, R. D. 1999 'A study of two-dimensional flow past an oscillating cylinder' *J Fluid Mech* 385, pp 255-286.
- [10] Drela, M. 1989, 'XFOIL: an analysis and design system for low Reynolds number airfoils', in *Low Reynolds Number Aerodynamics*. AIAA.